Motions of anisotropic particles: Application to visualization of three-dimensional flows

G. Gauthier,[a] P. Gondret, and M. Rabaud
Laboratoire Fluides, Automatique et Systèmes Thermiques,[b] *Bâtiment 502, Campus Universitaire, F-91405 Orsay Cedex, France*

(Received 9 December 1997; accepted 12 May 1998)

The aim of the paper is to get insight into flow patterns visualized by suspended anisotropic reflective particles. The motion of triaxial ellipsoids embedded in a three-dimensional flow, i.e., which cannot be reduced to a local plane Couette flow, is calculated. Both the asymptotic trajectory and the transient time to reach it are discussed. These results are used to simulate laser sheet visualizations of two classical three-dimensional flows (Taylor–Couette vortices and flow between rotating disks) where the particle history is shown to be negligible. The simulated visualizations are well compared to experimental ones but the paper addresses the fact that the legitimate question of what shows the visualization does not have a simple answer. Nevertheless, these results open the way for quantitative comparisons between computational fluid dynamics and experimental visualizations. © *1998 American Institute of Physics.* [S1070-6631(98)01409-3]

I. INTRODUCTION

For many years, nonaxisymmetric particles have been used at low concentrations to visualize liquid flows. These small particles, having almost the same density as the surrounding fluid, are oriented by the flow and can transmit or reflect incident light differently from place to place thus revealing the structure of the flow. Classically used particles are aluminum, coated mica flakes, or commercial products such as Iriodin[1] or Kalliroscope.[2] Nice examples of such visualizations can be found in the book of Van Dyke.[3] This visualization technique presents the advantage of giving strongly contrasted images in closed geometries and under permanent conditions even with very small particle concentration. It has been extensively used, e.g., for the study of the dynamic regimes of Taylor–Couette flow[4,5] or more recently for the study of small scales of turbulence.[6,7] Indeed, when the density of the particles is comparable to that of the fluid, the particles are advected at the fluid velocity. The particle Reynolds number, i.e., the one built with the particle size and shear rate, is then small even if the flow Reynolds number is large. Details about the size, density, and reflective index of the particles can be found in various textbooks or for Kalliroscope in the article of Matisse and Gorman.[8] The possible unwanted effects of adding such particles have been discussed by Dominguez-Lerma *et al.*[9] If one takes into account this broad utilization and the number of nice works based on this technique, it is surprising that very few authors were concerned by one essential question: ''What do these anisotropic particles show exactly?'' To our knowledge the only study trying to answer this question is the one of Savas,[10] who assumes that thin axisymmetric particles align themselves onto the ''stream surfaces'' in the case of plane Couette flow. He then calculates the reflected light intensity in the flow existing far above a rotating disk, where it can be approximated locally by an unidirectional flow. Under this assumption, it is possible to follow the orientation of a particle along a streamline. Subsequently, most authors dealing with other flow visualizations just mention that the flakes are oriented in the ''stream surfaces''[6,7,11] although this notion is not defined for nonunidirectional flow. Indeed, in general three-dimensional (3-D) flows, the flow cannot be reduced locally to a plane Couette flow. Even if the orientation motion of anisotropic particles in a viscous fluid has been extensively studied, most of the authors were concerned on the one hand by the possible effect on suspension rheology at larger concentration,[12] and on the other hand by the characterization of the particles by birefringence properties.[13] The aim of this paper is to compute the orientation motion of isolated nonaxisymmetric particles in a general 3-D flow in order to point out the link between the visualizations and the velocity fields.

In Sec. II we briefly recall the analytical results for the motion of axisymmetric particles. Section III is devoted to the numerical simulation of the motion of a triaxial particle in a general 3-D flow. Section IV deals with the simulation of the flow visualization with anisotropic particles and its comparison with experimental visualization for two classical stationary axisymmetric 3-D flows (Taylor–Couette flow and the flow between rotating disks with separated boundary layers).

II. MOTION OF AXISYMMETRIC ELLIPSOIDS

The first and fundamental work was done by Jeffery in 1922,[14] who analyzed the motion of one rigid isodensity ellipsoid in a general viscous flow. The particle is considered to be small enough so that the Reynolds number based on its

[a]Electronic mail: gauthier@fast.u-psud.fr; Telephone: 33-1 69 15 80 88; Fax: 33-1 69 15 80 60.
[b]Associated with Universities Pierre & Marie Curie and Paris-Sud and with CNRS (UMR 7608).

length and on the typical shear remains small. Brownian motion is neglected as any body forces. The first result of Jeffery is that, to the leading order, it is not necessary to take into account the flow modification around a particle and so the torques undergone by any isolated triaxial ellipsoid are the same as those given by the unperturbed velocity field. At each time, the motion of the particle is the sum of a translation and of an instantaneous rotation vector ω which governs the orientation of the particle. The components of this vector ω *in the frame of the particle* are:

$$\omega_1=\frac{b^2G_{3,2}-c^2G_{2,3}}{b^2+c^2},$$

$$\omega_2=\frac{c^2G_{1,3}-a^2G_{3,1}}{a^2+c^2}, \tag{1}$$

$$\omega_3=\frac{a^2G_{2,1}-b^2G_{1,2}}{a^2+b^2},$$

where the indices 1, 2, and 3 refer to an orthonormed frame of reference, called $\mathscr{S}$, built on the axes **a**, **b**, and **c** of the ellipsoid. The term $G_{i,j}=\partial V_i/\partial x_j$ is one of the nine terms of the velocity gradient tensor **G** which characterizes the flow in that frame. For a general 3-D flow this tensor has three nonzero eigenvalues.

To go further, Jeffery focuses on axisymmetric ellipsoids ($b=c$). In that case only one geometrical parameter, the aspect ratio $r=a/b$, is necessary to describe the particle. The case $r>1$ corresponds to prolate spheroids and $r<1$ to oblate spheroids. Later, Leal and Hinch[15] expressed the work of Jeffery in a more compact form. The orientation of the particle is then given by the time evolution of a unit vector **p** parallel to the particle symmetry axis **a**:

$$\frac{d\mathbf{p}}{dt}=\Omega\cdot\mathbf{p}+\frac{r^2-1}{r^2+1}[\mathbf{E}\cdot\mathbf{p}-\mathbf{p}\cdot(\mathbf{p}\cdot\mathbf{E}\cdot\mathbf{p})], \tag{2}$$

where Ω and **E** are, respectively, the vorticity tensor and the rate-of-strain tensor (respectively, antisymmetric and symmetric parts of the velocity gradient tensor **G**). Note that Eq. (2) is only valid in the frame $\mathscr{S}$ of the ellipsoid. The first term on the right-hand side is the usual rotation due to vorticity, the first term in brackets is the rotation induced by the elongational nature of the flow for a nonspherical particle ($r\neq1$), whereas the last term just ensures the norm conservation of **p**. So in Eq. (2), all the orientation dynamics is contained in the evolution tensor ξ:

$$\xi=\Omega+\frac{r^2-1}{r^2+1}\mathbf{E}. \tag{3}$$

In the case of a simple stationary shear flow of shear rate γ, Jeffery has shown that equations of motion can be integrated and that the particles experience periodic closed orbits with a period $T=(2\pi/\gamma)(r+1/r)$. This family of orbits is parametrized by a constant C ($0\leqslant C\leqslant\infty$) which comes from the initial orientation of the ellipsoid. Thus, a particle never forgets its initial orientation. For any initial orientation, the extremity of **p** describes a closed orbit around the vorticity axis (z axis) as follows: close to this axis if C is small or r large, and close to the shear plane (xOy plane) if C is large or r small (Fig. 1). A disk-like particle (r small) spends most of its time with **p** along the shear axis (y axis) whereas for a rod-like particle (r large) it is along the flow axis (x axis). In both cases, the particles flip rapidly, with the time scale $2\pi/\gamma$, in the shear plane. These motions have been checked quantitatively in the experiments of Goldsmith and Mason.[16]

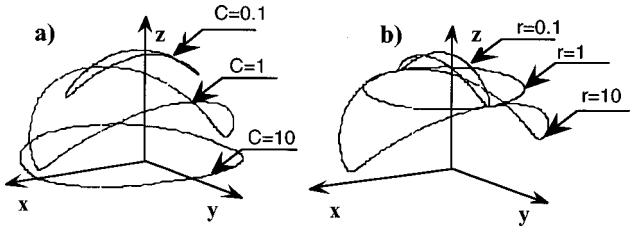

FIG. 1. A set of Jeffery orbits (trajectories of the extremity of **p** for an axisymmetric particle rotating in a plane Couette flow ($u_x=\gamma y$) for $C=0.1$, 1, and 10, and aspect ratio $r=10$ (a) and for $C=1$, and $r=0.1$, 1, and 10 (b). Analytical results and simulation (Sec. III A) are superimposed on these curves but cannot be distinguished.

The effect of Brownian motion on these orbits was investigated theoretically by Leal and Hinch[17] for such a plane Couette flow acting on spheroids (with r close to 1). For a diffusion constant of the orientation[18] low compared to the shear rate, these authors show that there exists a smooth selection process that slowly orients the particles in the vicinity of one particular Jeffery orbit selected by the value of the aspect ratio r. Thus, because of the Brownian forces, every particle slowly lose the memory of their initial orientation.

These Jeffery orbits are quite specific to the plane Couette flow. In 1962, Bretherton addressed the motion of an axisymmetric body in any three-dimensional flow.[19] As all the dynamics in the frame of the particle is contained in the evolution tensor ξ [Eq. (3)], it is sufficient to study the evolution of a vector $\hat{\mathbf{p}}$ which is parallel to **p** but does not conserve its norm. Being interested in the stationary orientation motion of the ellipsoid, Bretherton looks for the $\hat{\mathbf{p}}$ eigenvector of ξ. For any velocity field, the characteristic polynomial is of third order with real coefficients. Thus, there are either three real eigenvalues or a real and two complex conjugate ones and as the fluid is incompressible, the sum of the eigenvalues is zero. The nature of the eigenvalues determines the asymptotic trajectory of the axis of revolution, the transient time to reach it, and the period of rotation. When one of the real parts of the eigenvalues is larger than the two others, the vector **p** aligns in the direction of the corresponding eigenvector. Thus the particle will keep a constant orientation which depends on its aspect ratio r. If the two larger real parts of the eigenvalues are equal the dynamics depends on the imaginary parts. First, if they are zero the particle also evolves into a fixed direction which depends here on its initial orientation (this case has not been described by Bretherton). Second, if the imaginary parts are nonzero (thus they are equal and of opposite sign) the **p** axis rotates in a plane generated by the real and imaginary parts of the two corresponding complex conjugate eigenvectors. Finally, if the

three real parts of the eigen values are zero, the axis of revolution **p** describes a nonplanar closed curve that depends on its initial orientation. This case occurs only for purely rotational flow or plane Couette one. The case of Jeffery's orbits is just a particular case of this last category. In all cases the transient time τ is given by the inverse of the largest real part of the eigenvalues, whereas the period of rotation T is given by the inverse of the imaginary part.

Since these pioneering works, other effects have been taken into account: the time dependence of the flow,[20–22] large particle concentration,[23,24] deformable particles,[25,26] and inertia.[27] To our knowledge, the only papers dealing with nonaxisymmetric particles correspond to plane Couette flow.[28,29] These authors showed that this motion is composed of a rapid rotation around Jeffery orbits, and a slower periodic drift leading to a change of orbit. Recently it has been shown that chaotic drifts could exist in that case.[29]

III. MOTION OF TRIAXIAL ELLIPSOIDS

For a general triaxial ellipsoid, there is no theoretical prediction for its motion in a general 3-D flow. We then calculate this motion by using Jeffery's equations [Eq. (1)] in order to shed some light on trends that are useful for visualization.

A. Outline and validation of the calculation

In this section we assume a constant velocity gradient tensor $\mathbf{G}_0$ in the laboratory frame $\mathscr{L}_0$. As Eq. (1) gives the instantaneous rotation vector $\boldsymbol{\omega}$ in the frame of reference $\mathscr{L}$ of the particle, we first compute $\mathbf{G}$ in $\mathscr{L}$. At time t, knowing $\mathbf{G}$, we calculate $\boldsymbol{\omega}$ by Eq. (1). We compute by Euler stepping the new orientation of the particle using the rotation matrix $\mathbf{R}$ based on $\boldsymbol{\omega}$ and the time step Δt. From this new orientation at time $t+\Delta t$ we then compute the new tensor $\mathbf{G}'$ by the relation $\mathbf{G}'=\mathbf{R}^{-1}\mathbf{G}\mathbf{R}$ and the process is repeated for each time step. The time step Δt is small enough if $\Delta t \ll 1/\|\boldsymbol{\omega}\|$. In a Couette flow, a constant time step can be used and we choose $\Delta t = 0.01/\gamma$ in order to describe well the rapid flips. In a general 3-D flow, since $\mathbf{G}$ and hence $\|\boldsymbol{\omega}\|$ depend on the orientation, we must calculate at each instant the time step $\Delta t = 0.01/\|\boldsymbol{\omega}\|$.

We have first checked the computation for axisymmetric particles in a plane Couette flow: For various initial orientations of the particle and any tested aspect ratio ($0.1<r<10$), the agreement is perfect with the theoretical Jeffery's orbits (Fig. 1). We have also checked that the calculation for an axisymmetric ellipsoid in a general 3-D flow is in agreement with Bretherton predictions: For various random tensors $\mathbf{G}_0$, we observe that either **p** evolves in a fixed direction, or this vector rotates in a plane. Note that these two behaviors can also be obtained with the same flow (the same $\mathbf{G}_0$) but by varying the particle aspect ratio. In most cases long particles align themselves along fixed directions whereas disks rotate. In each case we checked that the eigenvalues indeed govern the corresponding asymptotic trajectory and the transient time to reach it.

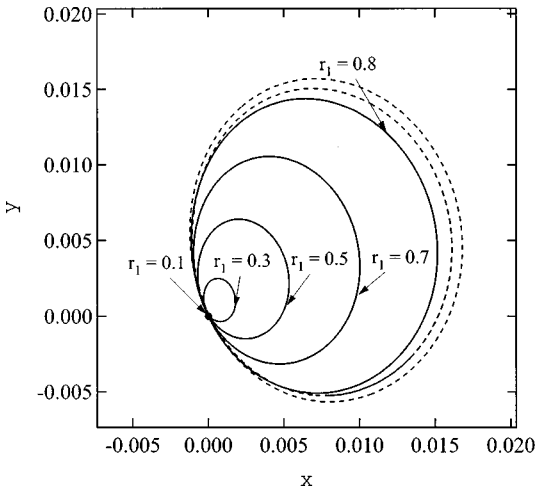

FIG. 2. Projection in the *xOy* plane of the extremity of the unit vector **p** for a nonaxisymmetric ellipsoid with various aspect ratio r_1 and fixed $r_2 = 0.1$ in a generic three directional flow. For $r_1 = 0.1$ (long prolate spheroid), the **p** direction is fixed (large point in $x=y=0$). For any r_1 value between 0.1 and 0.9 ($r_1 = 0.3,\ 0.5,\ 0.7,\ 0.8$) the projection corresponds to a unique closed curve (—) including the previous fixed point. The amplitude of the precession increases but remains small (note the magnified scale compared to unity). For $r_1 = 0.95$, the trajectory is biperiodic (---).

B. Behavior of nonaxisymmetric ellipsoids

For a non-axisymmetric ellipsoid, one can define two aspect ratios $r_1 = b/a$ and $r_2 = c/a$. Then Eq. (1) may be written as

$$\boldsymbol{\omega} = \begin{cases} \Omega_{3,2} + \dfrac{r_1^2 - r_2^2}{r_1^2 + r_2^2}\mathbf{E}_{3,2} \\ \Omega_{1,3} + \dfrac{r_2^2 - 1}{r_2^2 + 1}\mathbf{E}_{1,3} \\ \Omega_{2,1} + \dfrac{1 - r_1^2}{1 + r_1^2}\mathbf{E}_{2,1}. \end{cases} \tag{4}$$

We choose $a \geqslant b \geqslant c$, for which $r_2 \leqslant r_1 \leqslant 1$. All the simulations computed with different aspect ratios and different tensors $\mathbf{G}_0$ point out that even nonaxisymmetric ellipsoids reach an asymptotic trajectory after a transient time τ.

We first study the asymptotic trajectories of an ellipsoid which is gradually deformed from a long prolate spheroid to a thin oblate one. We thus vary b from c to a (r_2 is constant and r_1 varies between r_2 and 1). We study the trajectory of the extremity of a unit vector **p** parallel to the **a** axis (the largest one), which is the axis of revolution when $r_1 = r_2$. In Fig. 2, we present the projection of these trajectories in the plane *xOy* for a given tensor $\mathbf{G}_0$.[30] For each aspect ratio between $r_1 = 0.1$ and 0.9, the extremity of **p** precesses, but all the curves pass through one point and remain close to it (Fig. 2). The amplitude of the precession (measured as the square root of the area) increases linearly with the aspect ratio r_1 although the period T_p remains constant. Note that the precession amplitude is very small compared to unity meaning that the motion *of the greatest axis* is almost the same as for a prolate spheroid even when the ellipsoid is

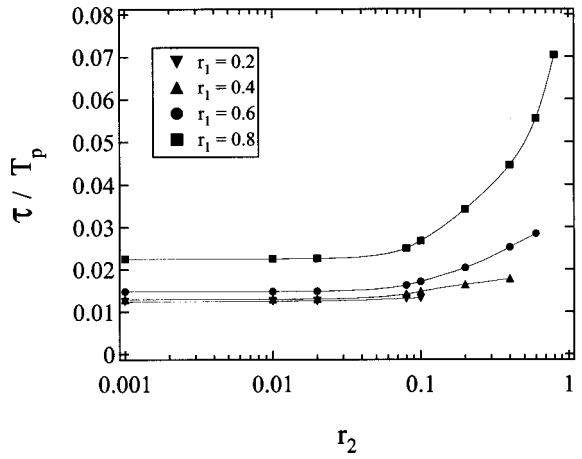

FIG. 3. For nonaxisymmetric ellipsoids of various aspect ratio r_1 (0.2, 0.4, 0.6, 0.8), evolution of the transient time τ to reach the asymptotic trajectory, vs the aspect ratio r_2 (logarithmic scale). The same generic three-dimensional velocity gradient $\mathbf{G}_0$ (Ref. 30) and the same initial orientation have been used. The time τ is made dimensionless by the asymptotic period of precession T_p of such particle in $\mathbf{G}_0$. The continuous lines are a guide for the eyes.

closer to an oblate one. For $r_1=0.95$, the trajectory becomes biperiodic and as r_1 approaches 1, the trajectory is more and more complicated. For $r_1=1$, we have checked that the trajectory of axis **c** is a circle in a particular plane: this agrees with Bretherton's predictions for an oblate spheroid. This description presented for $r_2=0.1$ remains true for other values of r_2.

An important result for the particle dynamics and thus for visualization purposes is the time necessary to reach its asymptotic trajectory. Such information for axisymmetric particles is given by the eigenvalues of ξ [Eq. (3)] and was also estimated by Weidman[31] in a plane Couette flow. We study the transient for nonaxisymmetric particles by varying r_1 and r_2. The evolution toward the asymptotic trajectory appears as exponential and we determine the characteristic time τ for one flow $\mathbf{G}_0$ and one initial particle orientation (Fig. 3). The main conclusion is that τ decreases for small r_1 or small r_2. Thus thin or long particles more rapidly reach their asymptotic trajectories. The transient time is short, typically of the order of a few percent of the period of rotation.

C. Concluding remarks for visualization purposes

We will now focus on general remarks useful for visualization with anisotropic particles.

On the one hand, the often encountered idea that thin particles are oriented in the ''stream surfaces''[6,7,11] only holds for, at least locally, plane Couette flow. Indeed, stationary orientation is only one of the possible asymptotic trajectories, and the others are time dependent trajectories: no stationary orientation is reached and the particles rotate with more or less complicated trajectories. The relation between visualizations and underlying velocity fields is thus not straightforward. In particular, since the particle orientation just gives access to one of the three eigenvectors of the velocity gradient tensor, it is not possible to reconstruct completely the velocity field from the observed light.

On the other hand, the motion of anisotropic particles in a general flow involves different time scales which have to be compared. Let us first present or recall these different time scales.

We have already introduced the period of rotation T of the particle on its asymptotic trajectory, and the transient time τ necessary for the particle to reach this asymptotic trajectory. When particles are advected in a real flow, they are submitted in their Lagrangian frame to a velocity gradient tensor **G** which is, in general, time dependent. This time dependence of **G** is due either to a time dependence of the Eulerian velocity field (unsteady flow) or to spatial variations of the steady velocity field, and one can so define a time scale of evolution of **G** in the frame of the particle and denote this time t_G. Since the anisotropic particles used in visualization are generally rather small, Brownian motion must be taken into account. Following Perrin,[18] one can define the time scale t_B for the particles to lose their orientation by diffusive process.

When the Brownian time t_B is much larger than the transient time τ of orientation, the fading effect of Brownian motion can be reasonably neglected; the particle motion is then deterministic and the particle history should in principle be taken into account as noted by Savas.[10] However, when the transient time τ necessary for the particle to reach its asymptotic trajectory is sufficiently small compared to the time scale t_G of evolution of **G** in the frame of the particle, an ''adiabatic'' approximation can be used. As shown in the preceding section, this condition will be all the more satisfied since particles are thin. Nevertheless the relevance of visualizations with anisotropic particles in turbulent flows[6,7] where t_G is certainly small may be questionable, especially for the characterization of the small scale structures of the flow.

IV. VISUALIZATION USING ANISOTROPIC PARTICLES

We will now use the results of the dynamics of nonaxisymmetric particles previously presented in order to simulate the light reflected by the particles in a real flow. In the simulation we consider monodisperse triaxial ellipsoids which do not interact and we neglect inertia, gravity, and Brownian motion as well as particle history. We will compare the reflected light computed from numerically simulated velocity fields with experimental visualizations. We choose to focus on two particular flows, which are three dimensional but axisymmetric and stationary, lighted by a radial laser sheet: the Taylor vortex flow and flow between rotating disks. However, the method presented here could be extended to any flow and any light disposition.

We first describe the experimental visualizations (Sec. IV A), then the simulated ones (Sec. IV B), and then a comparison between the two is made (Sec. IV C).

A. Experimental visualizations

Flow visualization using reflective flakes are commonly used in experiments. We performed experiments with Iriodin pigments[1] and Kalliroscope flakes[2] embedded in a water–glycerol mixture. Kalliroscope particles are platelets made of

FIG. 4. Photograph under microscope (100 μm $\times$ 100 μm) of a concentrated solution of Kalliroscope particles. Note the strong polydispersity and the low contrast due to the low relative reflective index in a water–glycerol mixture.

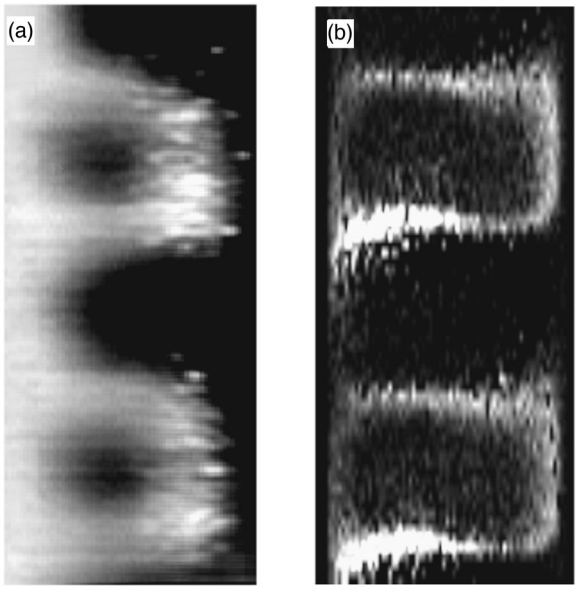

FIG. 5. Visualization of a radial laser sheet in a Taylor vortex flow: experiment (a) and simulation (b). The inner cylinder (to the left) rotates whereas the outer one (to the right) is fixed. The Taylor number of the flow is quite above the critical one corresponding to the appearance of Taylor vortices. In the experiment, $R_1=34$ mm, $R_2=36$ mm, $\Omega_1=0$, $\Omega_2=11.6$ rad s^{-1}, Ta $=9100$. In the simulation, $R_1=34$ mm, $R_2=35$ mm, $\Omega_1=0$, $\Omega_2=13.4$ rad s^{-1}, Ta$=6100$.

guanine (1.66 g cm^{-3} in density). A mean size of $30\times6\times0.07$ μm can be found in the literature as well as their reflective index of 1.85.[2,8] We have checked under a microscope that they are indeed very thin but they are also very polydisperse (Fig. 4). Iriodin pigments are platelets made of the natural mineral mica coated with a metallic oxide (3 g cm^{-3} in density) with a typical length less than 15 μm. Due to their small sizes, the sedimentation time in water is large (typically a few hours for 1 cm). We obtained similar images with both products but more contrasted ones with Kalliroscope. This may be related to our conclusion in Sec. III C since Kalliroscope flakes are much thinner than Iriodin ones. In the following, we focus on Kalliroscope visualizations. The particle concentration of the manufactured solution is not known. By an observation under microscope after dilution (Fig. 4) and also by weighting the dried part, we estimate the initial concentration to be 10^6 flakes/mm^3. Well contrasted visualizations are obtained for a volume fraction of 10^{-5}, leading to an averaged distance between the particles ten times greater than their largest size. The interactions between particles can then be neglected.[32]

In both experimental setups (concentric cylinders or parallel disks) the flow is mainly orthoradial and we use a radial laser sheet, of thickness 1 mm, transverse to the gap. Thus, the streamlines are almost perpendicular to the laser sheet. Figures 5(a) and 7(a) exhibit two typical experimental visualizations of such flows. Brighter domains are due to particles which are conveniently oriented or rotating when crossing the laser sheet in order to reflect light in the camera direction. The camera is oriented at 45° with respect to the normal to the sheet, in a plane generated by the normal to the sheet and a direction parallel (respectively, orthogonal) to the axis of rotation in the case of parallel disks (respectively, concentric cylinders). The angular aperture of the camera is of the order of 5°, and the exposure time is 1/25 s. Such laser sheet visualization is not classical in a closed geometry. Usually, this technique is used in open flows in order to observe the advection of a passive scalar.[33] In our flow configurations, information is only given by the orientation of the particles. Indeed, we checked that the reflected light intensity is homogeneous and no structures are observed when using isotropic particles such as Estapor.[34]

B. Simulated visualizations

Both flows were simulated by a CFD code in a radial plane. For the Taylor–Couette cell, the lattice is 34×40 for two wavelengths and a periodic boundary condition has been applied. Only the inner cylinder rotates and the Taylor number is Ta$=6100$, roughly three times the onset for the appearance of Taylor vortices.[5] For the rotating disks geometry, the simulation has been made with a 1024×64 lattice and under the same conditions as in the experiments: an aspect ratio $R/e=10$ and a Reynolds number $\mathrm{Re}=\Omega e^2/\nu=300$, below the onset of propagative circles or spirals but corresponding to separated boundary layers.[35]

In both cases, the velocity gradient tensor $\mathbf{G}_0$ is calculated at each lattice node. During the particle advection across the laser sheet, we check that the particle remains at the same node since the velocity is mainly orthoradial. Thus, within our resolution, the particle is submitted to a constant tensor $\mathbf{G}_0$ during its crossing. We also check that we can neglect particle history. In any node, we compute the transient time τ necessary for the particle to reach its asymptotic trajectory and compare this time to the advection time t_L across the sheet. The ratio τ/t_L is found to be small almost everywhere. Finally, we check that, since the particles are very thin, the real size is not a sensitive parameter for the asymptotic trajectory. We thus neglect polydispersity and assume monodisperse ellipsoids of axes $(a, b, c) = (30, 6,$

0.07) μm. For such thin particles the time t_B to lose their orientation with an angle equal to the camera aperture is, for our viscous fluid, of the order of 13 s. Thus, as $t_B \gg \tau$ and $t_B \gg t_L$, the Brownian motion has been also neglected.

At each node, we draw the orientation of one particle at random and we apply to it the torques it experiences during its advection time t_L across the laser sheet. We compute the proportion of time where the particle is well oriented in order to reflect light in the camera direction within the angular resolution of the camera. As we assume the flakes act as small mirrors, it is the orientation of the smallest axis **c** that we test. The light intensity at the corresponding node (or pixel) is then rescaled with the exposure time of the camera. However, when the period of rotation T of the particle on its asymptotic trajectory is not small compared to the advection time t_L across the laser sheet, the fraction of reflected light depends on the initial particle orientation when it enters the laser sheet. Thus, at each node corresponding to this case, we choose to draw several randomly oriented particles mapping the sphere unity and let them reach their asymptotic trajectory during a given time. In our simulation we draw at least 400 particles, this number corresponding to a mapping of the sphere of unit radius with the resolution given by the aperture angle of the camera ($\pm$ 5°).

Finally, we reconstruct a two-dimensional image by collecting the light intensity at each node (pixel). In order to compare quantitatively the results with the experiments, we introduce an *a posteriori* attenuation of the intensity due to light absorption of the fluid. We use a Beer–Lambert's[11] law consisting in an exponential attenuation with a constant scale z_0, neglecting here any effect of the orientation. The simulated images are presented in Figs. 5(b) and 7(b). These two images are in good agreement with the experimental ones [Figs. 5(a) and 7(a)] when the Beer–Lambert length z_0 is adjusted to 17 mm.

C. Comparison between simulation and experiment

For the Taylor–Couette flow, even if the simulation and the experiment are not at the same Taylor number, the same general features can be observed in Figs. 5(a) and 5(b): There is no reflected light in the core of the vortices and only the vortices of a given sign reflect light at their periphery. This simple visualization demonstrates clearly that the flakes are not ''pasted'' on the vorticity tubes contrary to the often encountered idea. Indeed, we have checked in the simulation that the light reflected for the Taylor vortices is generated by rotating Kalliroscope particles. The light intensity profiles corresponding to a vertical line in the middle of the gap are compared in Fig. 6(a). Although the brighter experimental domains are larger, the agreement between the two curves is rather good. The corresponding numerical radial velocity is given, in Fig. 6(b), for a comparison with the phase of the pattern.

For the flow between rotating disks, we distinguish three bright bands in both experimental and simulation visualizations (Fig. 7). For a more quantitative comparison, a vertical section of both pictures is shown in Fig. 8(a). The lighting being from above the light intensity decreases along the depth z due to the light attenuation. The two curves are in good agreement. A thin bright strip is localized close to each disk and a large bright band lies in the middle of the gap. The comparison between the visualization and the numerical velocity field [Fig. 8(b)] allows us to interpret each of the bright regions we observed. The bright strips close to the disks [Figs. 7 and 8(a)] correspond to the boundary layers where the azimuthal velocity varies rapidly along the depth [Fig. 8(b)]. These boundary layers, called Ekman and Bödewadt layers, are classical in such a flow configuration.[36] The thick bright center tongue [Figs. 7 and 8(a)] corresponds to a fluid core rotating nearly as a solid body, i.e., to a region where the azimuthal velocity is almost constant [Fig. 8(b)]. Note that the center large bright band between the disks is generated by particles having fixed orientation whereas the

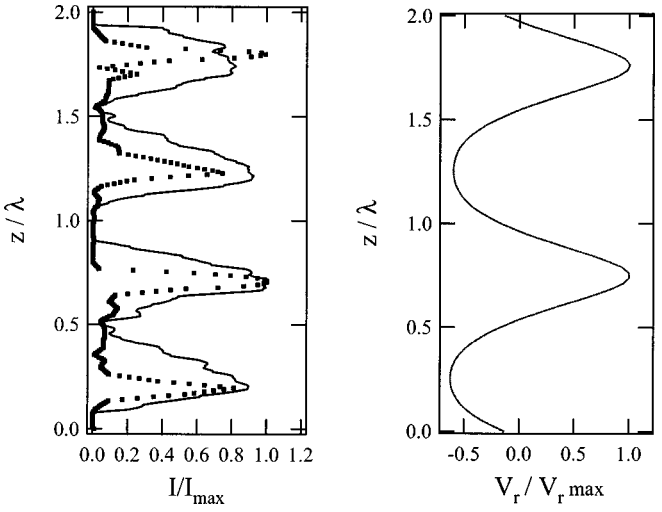

FIG. 6. (a) Normalized light intensity I/I_{max} as a function of z/λ (where λ is the wavelength) corresponding to a vertical profile at the radius $r=(R_2-R_1)/2$ of Fig. 5: experiment (—) and simulation (■). (b) Numerical normalized radial velocity V_r/V_{rmax} (—) as a function of the depth z/λ for a vertical profile at the same radius. Courtesy of H. Bellili.

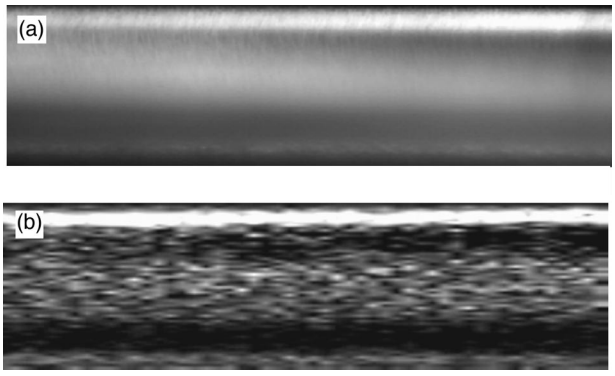

FIG. 7. Visualizations of radial laser sheet in the flow between two rotating disks: experiment (a) and simulation (b). In both cases, the axis of rotation is at the left and the top disk (together with the external wall) is rotating counterclockwise, when seen from above and the bottom disk is at rest. The radius of the disks is $R=140$ mm and the gap thickness is $e=14$ mm. Only a part of the cavity is presented ($r_{left}=0.4$ R, $r_{right}=0.6$ R). For both pictures the Reynolds number based on the gap thickness is $\mathrm{Re}=\Omega e^2/\nu \approx 300$. The experimental picture corresponds to an average over 20 pictures in order to increase contrast.

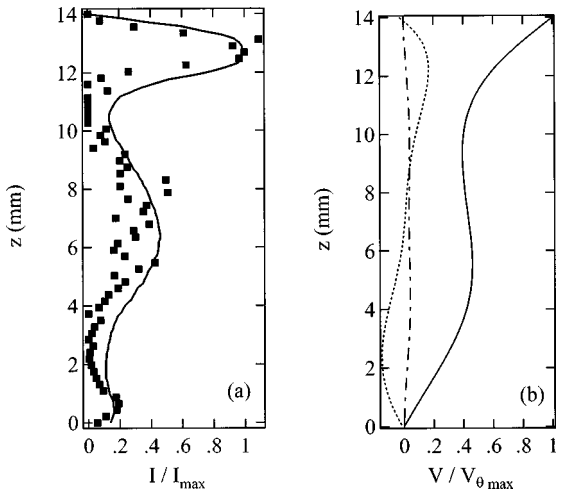

FIG. 8. (a) Normalized light intensity $I/I_{\max}$ as a function of the height z corresponding to a vertical profile of Fig. 7 at the radius of $r=0.57R$: experiment (—) and simulation (■). The experimental setup is lightened from above, so the intensity decreases with the depth. A Beer-Lambert attenuation law has been used in the simulation. (b) Numerical normalized velocity components as a function of the height z for a vertical profile at the radius $r=0.57R$: azimuthal velocity $V_\theta/V_{\theta\,\max}$ (—), radial velocity $V_r/V_{\theta\,\max}$ (---), and axial velocity $V_z/V_{\theta\,\max}$ (-·-). Courtesy of R. Jacques.

bright strips close to the disks are generated by rotating Kalliroscope particles. This rotating behavior is characteristic of 3-D flow. The boundary layers determined by our simulation of reflected light are well located and we have checked that they scale as $(\nu/\Omega)^{1/2}$ as expected in such a rotating setup.[37] This result was not observed in previous simulated visualizations of the flow over a rotating disk,[10] since they were based on a local plane Couette flow approximation.

V. CONCLUSION

In the present paper, we have investigated the orientation of a triaxial ellipsoid in general 3-D flows. Two main results have been exhibited. First, the nature of the asymptotic motion is controlled by the dynamics of its largest axis with a small precession induced by the nonaxisymmetry of the particle. Thus visualization using anisotropic particles is not an inverse method: From the observed light, it is not possible to reconstruct the velocity field. Second, the transient time is found to be smaller when one or the two aspect ratios are far from unity (long rods or thin disk). This value of the transient time compared to the time scale of the flow is important to determine whether or not the particle is an instantaneous tracer of the local property of the flow. These results have allowed us to build a simulation of the light reflected by anisotropic particles in general 3-D flows. We have applied this simulation in the case of laser sheet visualizations of two classical flows: Taylor vortices and flow between rotating disks. The agreement between the simulated visualizations and real ones is good, showing that the main parameters have been taken into account and that polydispersity, Brownian motion, and as well as particle history are not important. Moreover, in the case of the Taylor–Couette flow, we have shown that the particles are not ''pasted'' on the vortices, but that the observed light is due to rotating particles. For the flow between rotating disks, the thickness of the two boundary layers is correctly described in our simulated visualization. This shows clearly that the boundary layers can be tracked and that one can have confidence in thickness measurements with experimental visualizations using anisotropic flakes.

We believe that such simulations will allow a validation of a large number of experimental measurements, e.g., for the wavelength, the spatial or temporal growth rate of the structures, and the co- or contrarotating nature of vortices. In the near future, this simulation will allow us to determine quantitatively the relation between the light intensity and the amplitude of 3-D hydrodynamic instabilities.

ACKNOWLEDGMENTS

We would like to thank Professor E. J. Hinch and C. Allain for interesting discussions. We also thank R. Jacques and H. Bellili for computing the velocity fields necessary to perform our simulations of reflected light.

[1] Iriodin: Pigments sold by Merck Corporation.
[2] Kalliroscope Corporation, 264 Main Street, Box 60, Groton, MA 01450.
[3] M. Van Dyke, *An Album of Fluid Motion* (Parabolic, Stanford, 1982).
[4] D. Coles, ''Transition in circular Couette flow,'' J. Fluid Mech. **21**, 385 (1965).
[5] C. D. Andereck, S. S. Liu, and H. L. Swinney, ''Flow regimes in a circular Couette system with independently rotating cylinders,'' J. Fluid Mech. **164**, 155 (1986).
[6] K. W. Schwarz, ''Evidence for organized small-scale structure in fully developed turbulence,'' Phys. Rev. Lett. **64**, 415 (1990).
[7] J. D. Jacob and Ö. Savas, ''Experimental evidence for intense vortical structures in grid turbulence,'' Z. Angew. Math. Phys. **46**, S699 (1995).
[8] P. Matisse and M. Gorman, ''Neutrally buoyant anisotropic particles for flow visualization,'' Phys. Fluids **27**, 759 (1984).
[9] M. A. Dominguez-Lerma, G. Ahlers, and D. S. Cannell, ''Effects of 'Kalliroscope' flow visualization particles on rotating Couette-Taylor flow,'' Phys. Fluids **28**, 1204 (1985).
[10] Ö. Savas, ''On flow visualization using reflective flakes,'' J. Fluid Mech. **152**, 235 (1985).
[11] M. Sorrention and S. G. Mason, ''Rheo- and electro-optical behavior of platelets,'' J. Colloid Interface Sci. **41**, 178 (1972).
[12] J. Happel and H. Brener, *Low Reynolds Number Hydrodynamics* (Martinus-Nijhoff, Dordrecht, 1973).
[13] T. G. M. Van de Ven, *Colloidal Hydrodynamics* (Academic, London, 1989).
[14] G. B. Jeffery, ''The motion of ellipsoidal particles immersed in a viscous fluid,'' Proc. R. Soc. London, Ser. A **102**, 161 (1922).
[15] L. G. Leal and E. J. Hinch, ''The rheology of a suspension of nearly spherical particles subject to Brownian rotations,'' J. Fluid Mech. **55**, 745 (1972).
[16] H. L. Goldsmith and S. G. Mason ''Particle motions in sheared suspensions XIII. The spin and rotation of disks,'' J. Fluid Mech. **12**, 88 (1962).
[17] L. G. Leal and E. J. Hinch, ''The effect of weak Brownian rotations on particles in shear flow,'' J. Fluid Mech. **46**, 685 (1971).
[18] F. Perrin, ''Mouvement brownien d'un ellipsoïde,'' J. Phys. Radium **5**, 497 (1934).
[19] F. P. Bretherton, ''The motion of rigid particles in a shear flow at low Reynolds number,'' J. Fluid Mech. **14**, 280 (1962).
[20] A. J. Szeri, S. Wiggins, and L. G. Leal, ''On the dynamics of suspended microstructure in unsteady, spatially inhomogeneous, two-dimensional fluid flows,'' J. Fluid Mech. **228**, 207 (1991).
[21] A. J. Szeri, W. J. Milliken, and L. G. Leal, ''Rigid particles suspended in time-dependent flows: Irregular versus regular motion, disorder versus order,'' J. Fluid Mech. **237**, 34 (1992).
[22] A. J. Szeri, ''Pattern formation in recirculating flows of suspensions of orientable particles,'' Philos. Trans. R. Soc. London, Ser. A **345**, 477 (1993).
[23] G. G. Lipscomb and M. M. Denn, ''The flow of fiber suspensions in

complex geometries,'' J. Non-Newtonian Fluid Mech. **26**, 297 (1988).
[24]A. Mongruel and M. Cloître, ''Extensional flow of semi-dilute suspensions of rod-like particles through an orifice,'' Phys. Fluids **7**, 2546 (1995).
[25]W. L. Olbricht, J. M. Rallison, and L. G. Leal, ''Strong flow criteria based on microstructure deformation,'' J. Non-Newtonian Fluid Mech. **10**, 291 (1982).
[26]A. J. Szeri and L. G. Leal, ''Microstructure suspended in three-dimensional flows,'' J. Fluid Mech. **250**, 143 (1993).
[27]C. K. Aidun and E. Ding, ''Computational analysis of coating suspension,'' Proceedings of the Second European Coating Symposium, Strasbourg, 1997, edited by P. Bourgin and H. G. Wagner (Strasbourg, in press).
[28]E. J. Hinch and L. G. Leal, ''Rotation of small nonaxisymmetric particles in a simple shear flow,'' J. Fluid Mech. **92**, 591 (1979).
[29]A. L. Yarin, O. Gottlieb, and I. V. Roisman, ''Chaotic rotation of triaxial ellipsoids in simple shear flow,'' J. Fluid Mech. **340**, 83 (1997).
[30]The tensor $\mathbf{G}_0$ has been chosen in order to fix the asymptotic stationary orientation of **p** perpendicular to the plane *xOy* when $r_1=r_2=0.1$ (long prolate spheroid). The corresponding values are: $G_{11}=-12$, $G_{12}=-131$, $G_{13}=1/13$, $G_{21}=47$, $G_{22}=7$, $G_{23}=-16/29$, $G_{31}=-25/13$, $G_{32}=-100/29$ and $G_{33}=5$.
[31]P. Weidman, ''On the spin-up and spin-down of a rotating fluid. Part 2. Measurement and stability,'' J. Fluid Mech. **77**, 709 (1976).
[32]S. Kim and S. Karrila, *Microhydrodynamics, Principles and Selected Applications* (Butterworth–Heinmann, Boston, 1991).
[33]W. Merzkirch, *Flow Visualization* (Academic, New York, 1987).
[34]Estapor, latex particles sold by Prolabo (Rhône-Poulenc Corporation).
[35]G. Gauthier, Ph. Gondret, and M. Rabaud, ''Patterns between rotating disks,'' Dynamics Days, Lyon, 10-13 July 1996; L. Schouveiler, P. Le Gal, and M.-P. Chauve, ''Spiral and circular waves in the flow between a rotating and a stationary disk,'' to be published in Exp. Fluids.
[36]A. Sirivat, ''Stability experiment of flow between a stationary and a rotating disk,'' Phys. Fluids A **3**, 2664 (1991).
[37]G. Gauthier, Ph. Gondret, and M. Rabaud, ''Visualisation d'écoulements entre deux disques tournants,'' in Visualization and Image Processing in Fluid Mechanics), Saint-Louis (France), edited by Paul Smigielski (Tehna, Toulouse, 1997).